AIAA JOURNAL
Vol. 36, No. 3, March 1998

Confined Coaxial Nozzle Flow with Central Lobed Mixer at Different Velocity Ratios

S. C. M. Yu* and X. G. Xu†
Nanyang Technological University, 639798 Singapore

In a continuing effort to study the mixing enhancement by streamwise vorticity, time-average velocity measurements of turbulent, confined, coaxial nozzle flows with a central four-lobe forced mixer were obtained by a two-component fiber-optic laser-Doppler anemometer at a Reynolds number of 5.1×10^4 (based on the baseline circular nozzle diameter D_i = 30 mm and bulk mean velocity U_r of the two streams at 1.7 m/s). Ratios of the annular mean to the core mean velocity (λ) were kept at 0.4, 1.1, and 2.0, respectively. Results showed that the mixing processes were greatly enhanced by the formation and interaction of the azimuthal and streamwise vorticities. In particular, the deformation and the subsequent stretching of the azimuthal vortices shed at the nozzle walls by the streamwise vortices played a crucial role in the mixing processes. The higher-speed stream appeared to determine the form of mixing downstream. At λ = 2.0 and 1.1, the generation of the streamwise vorticity by the lobes and that from the gap between the lobe nozzle peaks and the inner annular wall enhanced the mixing between the two coflowing streams as well as with the surrounding still fluid. At λ = 0.4, the generation of vorticity was by only the geometry of the lobe, which shed streamwise vorticity that was confined radially within each lobe as the flow traveled downstream. Mixing between the central stream and the surrounding fluid was better than that between the two coflowing streams. For all of the cases considered, streamwise vortices were dissipated within $6D_i$ from the nozzle exit plane. Finally, attempts were made to identify the role of streamwise and azimuthal vorticities using the inviscid vortex dynamics.

Nomenclature

D_i = inner circular nozzle diameter at 30 mm
D_0 = annular nozzle diameter at 60 mm
H = boundary-layer shape factor, δ^*/Θ
k = turbulent kinetic energy, $\frac{1}{2}(u^2 + v_r^2 + v_\theta^2)$
Re = Reynolds number, $U_r D_i/\nu$ equal to 5.1×10^4
Re_Θ = Reynolds number based on the momentum thickness
U, u' = streamwise mean and the corresponding rms velocities
U_r = bulk mean velocity for the two streams
U_s = secondary mean velocity, $\sqrt{(V_r^2 + V_\theta^2)}$
V_r, v_r' = radial mean and the corresponding rms velocities
V_θ, v_θ' = circumferential mean and the corresponding rms velocities
x, r, θ = streamwise, radial, and circumferential directions (cylindrical coordinates)
x, y, z = streamwise, horizontal, and vertical directions (Cartesian coordinates)
Γ = overall circulation
δ^* = displacement thickness, mm
Θ = momentum thickness, mm
λ = ratios of the annular mean to the core mean velocity
ν = kinematic viscosity
Ω_x = streamwise vorticity
Ω_θ = azimuthal vorticity

Introduction

THE turbulent mixing of coaxial jets has direct relevance to furnaces and combustors and, largely for this reason, has been investigated extensively by many authors, for example, Durao and Whitelaw,[1] Ribeiro and Whitelaw,[2,3] Ko and Kwan,[4] Kwan and Ko,[5] and Champagne and Wygnanski.[6] Through extensive hot-wire and laser-Doppler anemometry measurements, the authors of Refs. 1–6 concluded that a coaxial jet can achieve the self-preserving state faster than a single jet. The dividing mechanism between the two coflowing streams provided conditions for vortex shedding and thereby enhanced their mixing.

The streamwise vortices generated in a jet, in addition to the azimuthal (or ring type) vortices, have been found to mix fluid streams even more efficiently. As pointed out in the investigations of Zaman,[7,8] both the azimuthal and streamwise vorticities are of equal importance to the jet mixing process and they are not independent of each other. The distortion of azimuthal vortex structures may lead to streamwise vortices under certain conditions. The streamwise vortices can be generated by many methods, for example, by installing small vortex generators or tabs immediately upstream of the trailing edge or by having a corrugated trailing-edge profile, i.e., a lobed nozzle, for the inner jet. The former have been examined extensively before; a great many details regarding mixing tabs can be found in the works by Zaman[8] and Zaman et al.[9] Generating the streamwise vortices using a lobed mixer and investigating the nature of these structures and their mixing enhancement capabilities are, thus, the focus of the present investigation.

Applications of a lobed mixer in the turbofan engine exhausts and ejectors have been studied extensively in the last decade (Fig. 1). The rapid mixing of the core and the bypass flows can achieve both noise reduction and thrust augmentation. Both the lobe shape and the lobe penetration angle were the important parameters to determine the effectiveness of mixer performance.[10,11] Streamwise vorticity was essentially inviscidly generated, and its strength should be higher when the lobe penetration region consists of straight parallel sidewalls.[12,13]

Almost all of the previous investigations in lobed forced mixer flows were conducted with a two-dimensional flow situation where the mixer was modeled as a splitter plate with corrugated trailing edge. The water-tunnel visualization tests[10] revealed that both the streamwise vorticity and the accompanying increase in interfacial area (relative to a flat plate) were significant contributors to the mixing enhancement. The enhancement of mixing was even stronger at higher velocity ratios. The structure of the flow behind the lobed mixer followed a three-step process by which the streamwise vortex cells were formed, intensified, and then breakdown. Most intense mixing seemed to occur at the third region. Varying the velocity

Received June 23, 1997; presented as Paper 97-1811 at the AIAA 28th Fluid Dynamics Conference, Snowmass Village, CO, June 29–July 2, 1997; revision received Oct. 20, 1997; accepted for publication Oct. 29, 1997.

*Senior Lecturer, Thermal and Fluids Engineering Division, School of Mechanical and Production Engineering. Member AIAA.
†Research Student, Thermal and Fluids Engineering Division, School of Mechanical and Production Engineering.

ratio across the lobe could cause a shift in the locations of these three regions.[11]

Although the results obtained from the experiments of a two-stream mixing flow situation have revealed many important aspects on the mixing characteristics of forced mixers, many practical applications of the lobed mixer are in the form of coaxial nozzle, where the flows considered should also include the mixing with the surrounding stagnant environment. Thus far, detailed velocity measurements obtained in a lobed mixer nozzle flow environment appear to be very scarce. Only the measurements of Belovich and Samimy[14] are known to the authors. Their investigations were conducted in an unconfined environment including detailed flow visualization studies.[14] Thus, the objectives of the present study are twofold. The first is to study the evolution of the streamwise vortex structure development and the corresponding impact on mixing processes in a confined environment. The second objective is to provide detailed velocity measurements suitable for a critical assessment of different turbulence models proposed to predict this type of industrial flow. Of particular note is the earlier work by the present authors on the measurements in coaxial nozzle flows with different central lobe configurations at velocity ratios less than 1 due to its relevance to certain types of combustor and turbofan exhausts systems.[15] The present measurements extend the existing measurements to include other velocity ratios to aid understanding of the flow behavior of such flows. Mean flow and turbulence measurements were made on fine crossplane grids across the wake region and to within six diameters (inner) downstream of the trailing edge using a two-component laser-Doppler anemometer. Attempts will also be made to examine the role of the azimuthal and streamwise vorticities at various velocity ratios using inviscid vortex dynamics.

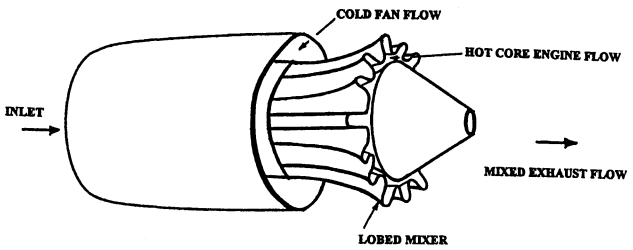

Fig. 1 Application of lobed nozzle in a turbofan engine exhaust.

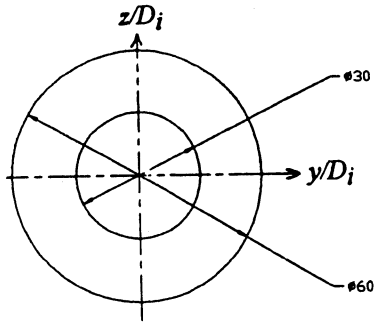

a) Baseline coaxial nozzle (end view)

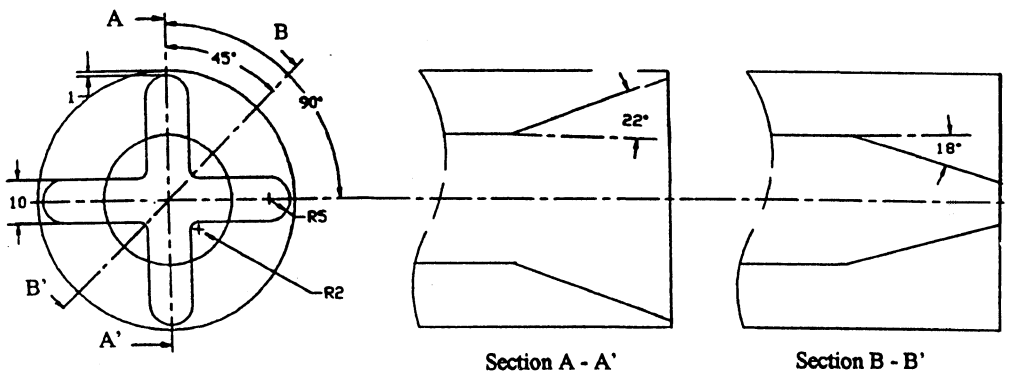

b) Four-lobe central nozzle (end view) **c) Four-lobe central nozzle (side view)**

Fig. 2 Coaxial nozzle configurations under investigation (all dimensions in millimeters, wall thickness = 1.5 mm).

The following section briefly describes the experimental setups including the laser-Doppler anemometer for obtaining velocity measurements. It is followed by the presentation and discussion of the results. The paper ends with a summary of more important findings.

Flow Configuration and Instrumentation

The water-tunnel facility used in the present investigation was the same as that described in Ref. 15. A coaxial contraction cone of area ratio 10:1 (for both the inner and outer cones) caused the flow to accelerate before discharging into a transparent rectangular test section of 400 × 400 × 1000 mm^3. Velocity difference between the inner and outer nozzles was achieved by incorporating screens and wire meshes either at the central or the annular nozzle. The flow passes through the transparent test section and settles at the sump tank (1000 × 1000 × 1000 mm^3) located at the end of the test section.

Figures 2a and 2b provide the detailed dimensions of central lobed nozzle and the baseline circular nozzle. The nozzles were manufactured of fiberglass and have wall thicknesses of 1.5 mm. The circular nozzle was intended for use as a baseline reference case where generation of streamwise vorticity was not expected. The central lobed nozzle has four lobes and the penetration angle from the core to the annular nozzle is 20 deg, whereas the penetration angle from the annular nozzle to the core is 18 deg. (It was found in Ref. 15 that flow separation would occur at the lobe troughs if the central nozzle had more than four lobes. To avoid complication to the subsequent analysis of the flow using inviscid vortex dynamics, the four-lobe central nozzle was chosen for study here.) The area of the central nozzle at the exit plane is 1057 mm^2, which provides an area ratio (outer to inner) of approximately 2.6 to 1.

For both cases considered the annular nozzle has a diameter of 60 mm. There is also a small gap of 1 mm between the peaks of each lobe and the inner wall of the outer nozzle.

Laser-Doppler Anemometer

A four-beam two-component fiber-optic laser-Doppler anemometer together with a 300-mW argon air-cooled laser operating in a backward scattered mode were used to measure respective velocity components. A focusing lens of 400 mm provided a measuring probe volume of 0.09 × 0.09 × 1.31 mm^3 in the vertical direction and

$0.085 \times 0.085 \times 1.24\ mm^3$ in the horizontal direction. The fiber-optic probe was mounted on an automated three-dimensional traversing system with an accuracy of ±0.01 mm. Bragg shifting of frequency up to 2 MHz (on each channel) was used to avoid directional ambiguity. The Doppler signals were detected by photomultipliers and processed by the Automatic Burst Correlators (TSI IFA 750). The natural contaminants inside the water were sufficient to produce high-validation data rate. Except at some regions immediately behind the trailing edge, data rates of 500–1000 Hz were normally obtainable. At each measuring point, the mean velocities, the rms of the velocity fluctuations, and the Reynolds shear stresses were determined from populations of more than 5000 (on each channel) samples together with a coincidence window of 1 μs.

The possible sources of uncertainty associated with the measurements of velocity were considered in detail by Xu[16] and include aspects of optical arrangements, the signal, and data processing systems. The velocity fluctuations occurred at moderate frequency so that the natural contaminants were able to follow the flow; thus, no inaccuracy should be attributed to this source. Similarly, the signal processing system is unlikely to have given rise to important uncertainties (maximum 0.5% based on manufacturer's specifications). Nevertheless, statistical effects together with velocity gradient broadening due to finite dimensions of the measuring volume were responsible for maximum uncertainties in the ensemble-averaged mean and rms velocities of 1% and 2% (normalized by U_r), respectively. All of these sources were estimated based on a 95% confidence level.

Measurements of the three orthogonal mean velocities U, V_r, and V_θ and their corresponding rms fluctuations u', v_r', and v_θ' were acquired in the projected area corresponding to one lobe, i.e., half of the cross-sectional area, as shown in Fig. 2b and at downstream locations where $x/D_i = 0.25$, 0.5, 1, 2, 3, 4, 5, and 6. For the centerline velocities, measurements were obtained until $x/D_i = 10.0$. At each station, there were about from 500 (at stations near the jet exit) to 900 (far downstream) measuring points at each lobe. Symmetry of the flow about the horizontal and vertical axes at the exit plane was within 5% based on the calculations of the mass flux.

The streamwise component of the vorticity $[\Omega_x = (\partial V_r/r\partial\theta) - (\partial V_\theta/\partial r)]$ was calculated based on a third-order polynomial fit to the V_θ and V_r measurements. The overall circulation was determined by obtaining the surface integral of the streamwise vorticity field at each half-lobe, i.e., a quarter of the cross-sectional area (also see Fig. 2).

Initial Conditions

The parameters for the velocity profiles measured at $x/D_i = 0.05$ for the baseline coaxial jet for the three velocity ratios are shown in Table 1. The shape factors for all of the cases showed that the boundary layers were turbulent. Streamwise turbulence level outside the boundary-layer region at the core and the annular section had maximum values of 1.0% and 1.2%, respectively.

Table 1 Characteristics of exit boundary layers (coaxial nozzle configuration)

Variable	Inner jet	Outer jet (internal)	Outer jet (external)
		$\lambda = 2.0$	
δ^*, cm	0.47	0.40	0.40
Θ, cm	0.27	0.24	0.25
H	1.85	1.67	1.6
Re_Θ	303.3	569.6	593.3
		$\lambda = 1.1$	
δ^*, cm	0.43	0.41	0.41
Θ, cm	0.28	0.26	0.27
H	1.54	1.57	1.52
Re_Θ	471.8	438.1	455
		$\lambda = 0.4$	
δ^*, cm	0.35	0.49	0.49
Θ, cm	0.25	0.29	0.3
H	1.4	0.69	1.63
Re_Θ	505.5	260.6	269.6

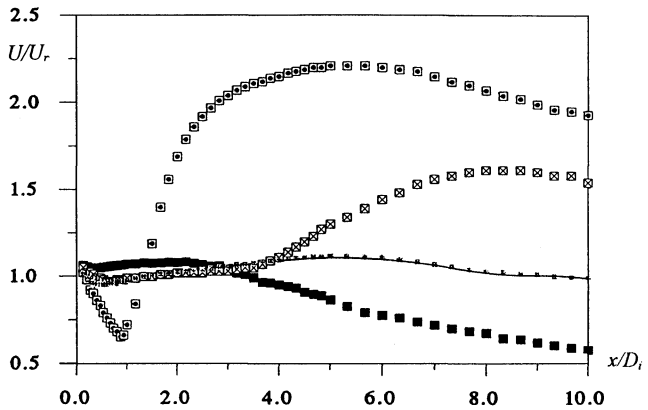

Fig. 3 Variation of centerline streamwise mean velocity with downstream distance: □, λ = 2.0; ▲, λ = 1.1; ■, λ = 0.4; and ⊠, baseline coaxial nozzle.

Results and Discussion

Centerline Streamwise Mean Velocity

Figure 3 shows the centerline velocity distribution for the three velocity ratios. The distributions were characterized by three different regions: the initial reduction from the exit plane was followed by an increase to a peak and a decrease followed thereafter. The reduction for the velocities in the first diameter downstream of the nozzle exit plane had the fastest rate for $\lambda = 2.0$, indicating a higher strength of secondary flow was being generated in the outward radial direction by the central lobed nozzle. After $x/D_i = 1$, the annular flow started to influence the velocity at the centerline, which showed an increase in magnitude. The growth rate was higher for $\lambda = 2.0$ than for the other two cases. This effect was mainly associated with the strength of the streamwise vortices shed by the lobes (the rate at which the annular fluid was being convected toward the centerline). Note that, in the unconfined situation of Belovich and Samimy,[14] the inward secondary flow was not as strong. The peak for the respective cases appeared at different locations with the lowest λ located at the closest position to the trailing edge. A faster reduction rate after the peak was, however, found at $\lambda = 0.4$ indicating that the secondary flow in the outward radial direction became higher. Thus, higher strength of secondary flow was actually generated by the higher-speed stream for both $\lambda = 0.4$ and 2.0. The results are contrasted to those found in the two-dimensional lobed mixer, where the lower-speed stream usually generated higher secondary flows.[13] For the case of $\lambda = 1.1$, the increasing rates before and after the peak were nearly the same, indicating the secondary flow strength was almost equal for both streams.

The length of the potential core for the baseline circular nozzle at $\lambda = 2.0$ was about $8.0D_i$, compared with $3.0D_i$ for the lobed nozzle (also shown in Fig. 3). This was an obvious indication of the increased mixing for the lobed nozzle causing the two coflowing streams to interact sooner.

Development of the Streamwise and Secondary Mean Velocities

Contours of the streamwise mean velocity and the corresponding secondary flow velocity vectors at four selected downstream stations from the exit plane are presented in Figs. 4–6. For all three of the velocity ratios considered (Figs. 4a and 4b, 5a and 5b, and 6a and 6b), a pair of counter-rotating vortices was formed downstream of the trailing edge, from $x/D_i = 0.5$ to 1.0, with the vortex core located at around the midpoint of the straight parallel sidewall. As may be expected from the centerline velocity measurements, the strength of the secondary flow was higher at the higher speed stream for $\lambda = 0.4$ and 2.0. At $\lambda = 1.1$, the strength of the secondary flow was nearly the same at both streams.

At $x/D_i = 1.0$ and for $\lambda = 2.0$ (Fig. 4b), streamwise mean velocity contours at the annular wall region began to shift radially outward along the plane of symmetry. The migration became more noticeable by $x/D_i = 2.0$ (Fig. 4c) such that the stretching of the contour lines along the plane of symmetry had actually penetrated into the surrounding area occupied by the still fluid. Similar effects, however, were not observed at $\lambda = 0.4$ (Fig. 6b) and were less

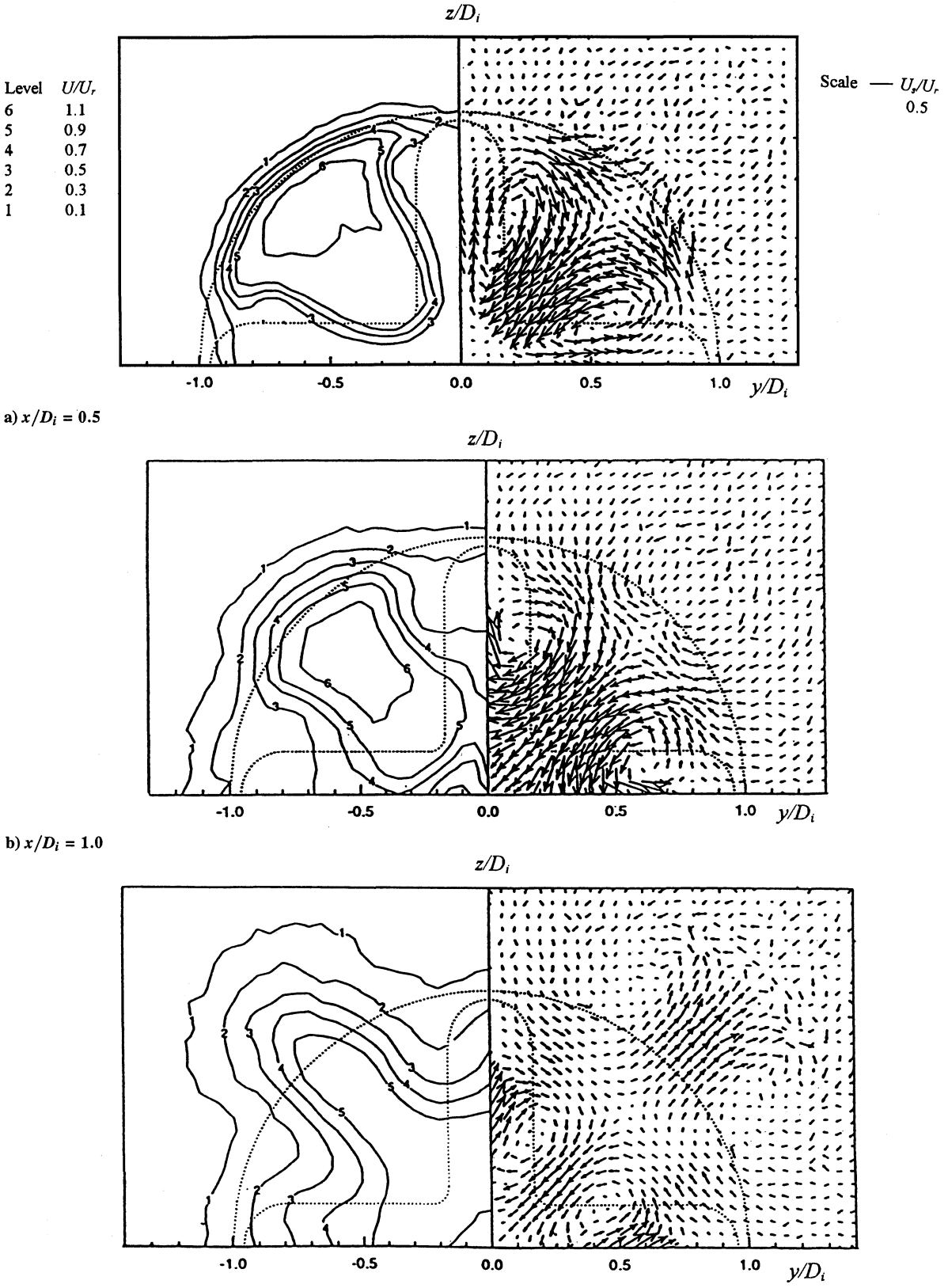

Fig. 4 Contours of the normalized streamwise mean velocity at successive downstream station for $\lambda = 2.0$.

obvious at $\lambda = 1.1$ (Fig. 5b). The streamwise mean velocity contours for $\lambda = 1.1$ and 0.4 also had penetrated into the surrounding fluids but mainly in the directions along the lobes (Figs. 5c and 6c). This appeared to be the direct result of a higher secondary flow generated by the higher-speed stream.

Based on the findings of Ref. 15, the radial migration of the velocity contours along the plane of symmetry for the $\lambda = 2.0$ case was due to streamwise vorticity generated from the gap between the lobe peaks and the inner wall of the annular nozzle. It was further observed that, when the gap was above $0.15D_i$, no streamwise vorticity would be generated. The same observation, however, was not found in the measurements of Belovich and Samimy.[14] In their case, the gap between the central lobed nozzle and the annular jet was about half of the inner nozzle diameter. By $x/D_i = 4.0$, the strength of the secondary flow velocity reduced substantially, and the corresponding streamwise mean velocity distribution for

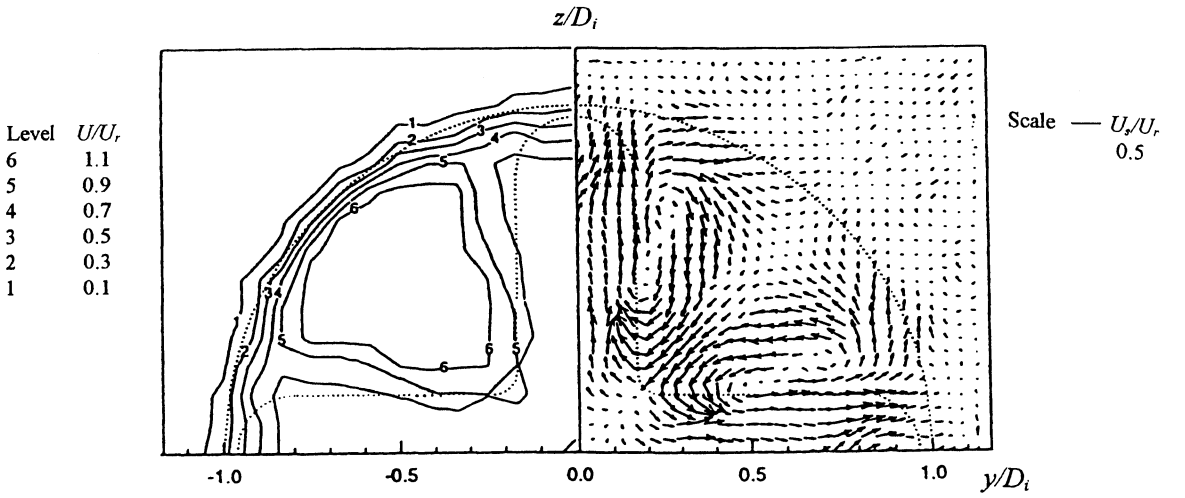

a) $x/D_i = 0.5$

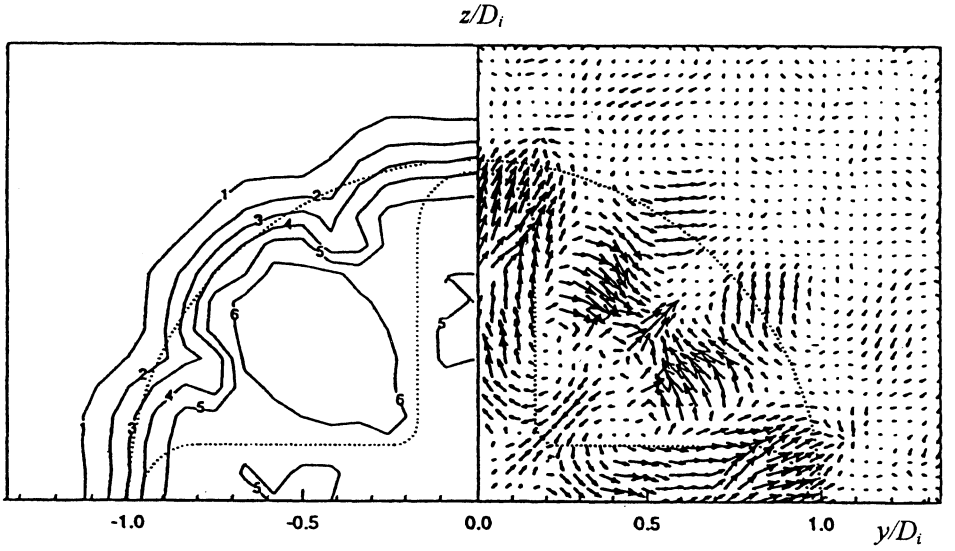

b) $x/D_i = 1.0$

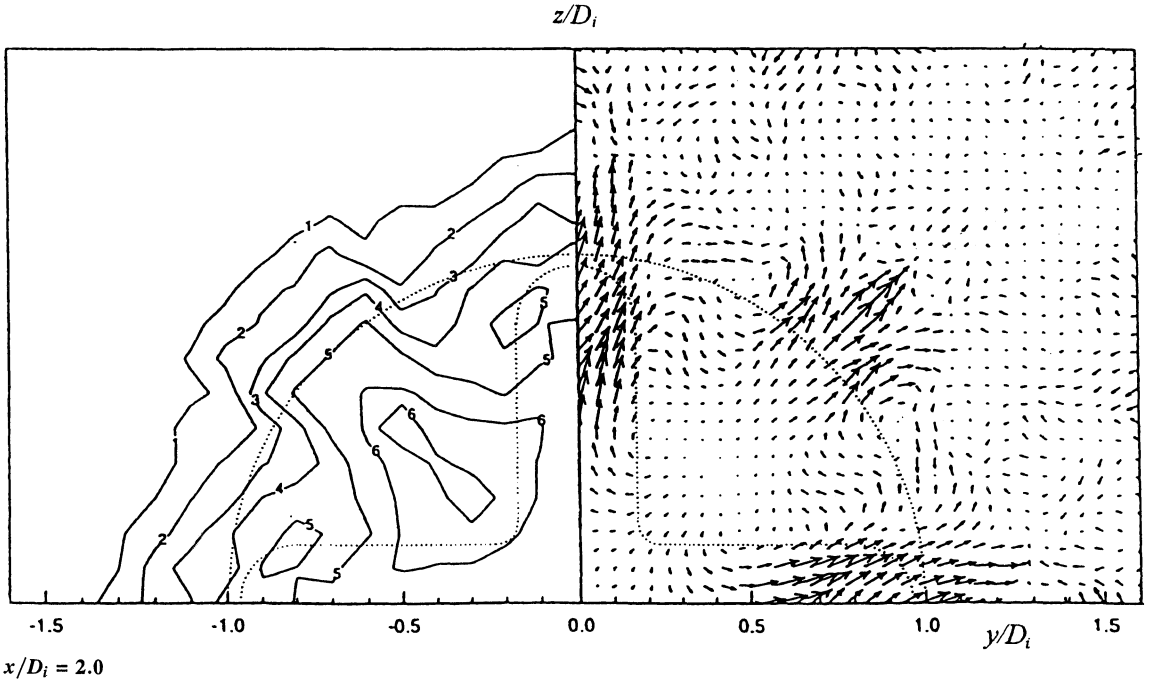

c) $x/D_i = 2.0$

Fig. 5 Contours of the normalized streamwise mean velocity at successive downstream station for $\lambda = 1.1$.

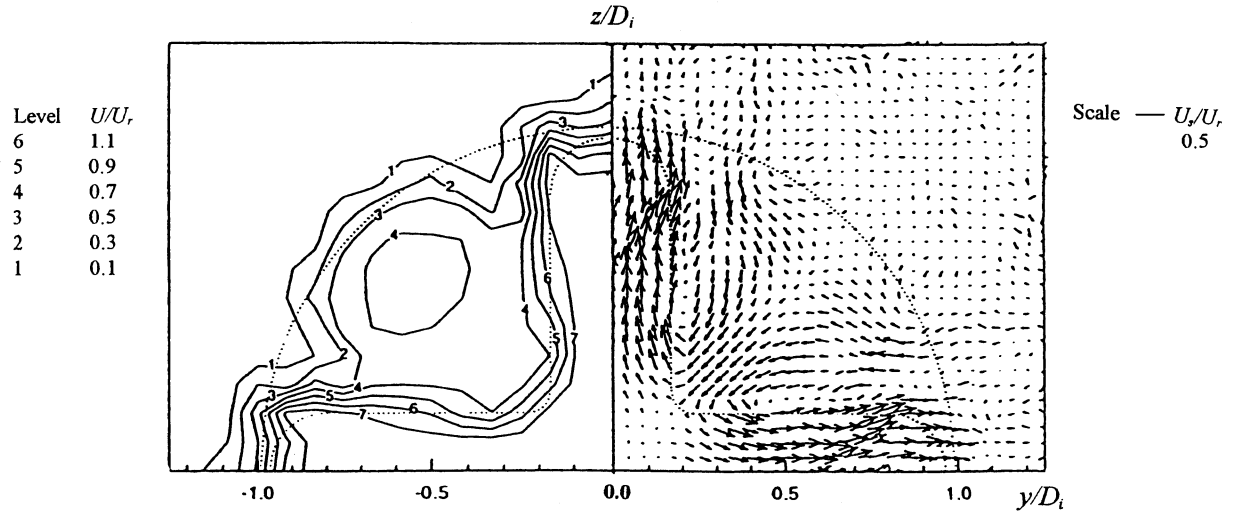

a) $x/D_i = 0.5$

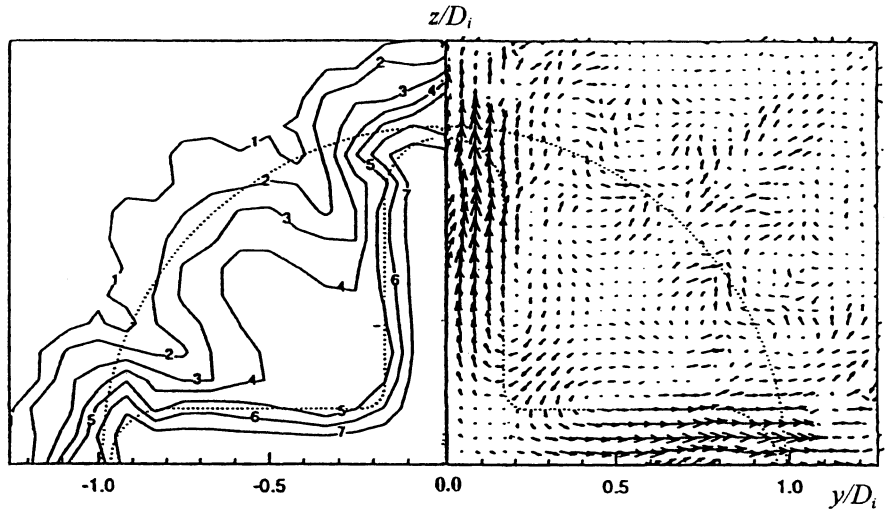

b) $x/D_i = 1.0$

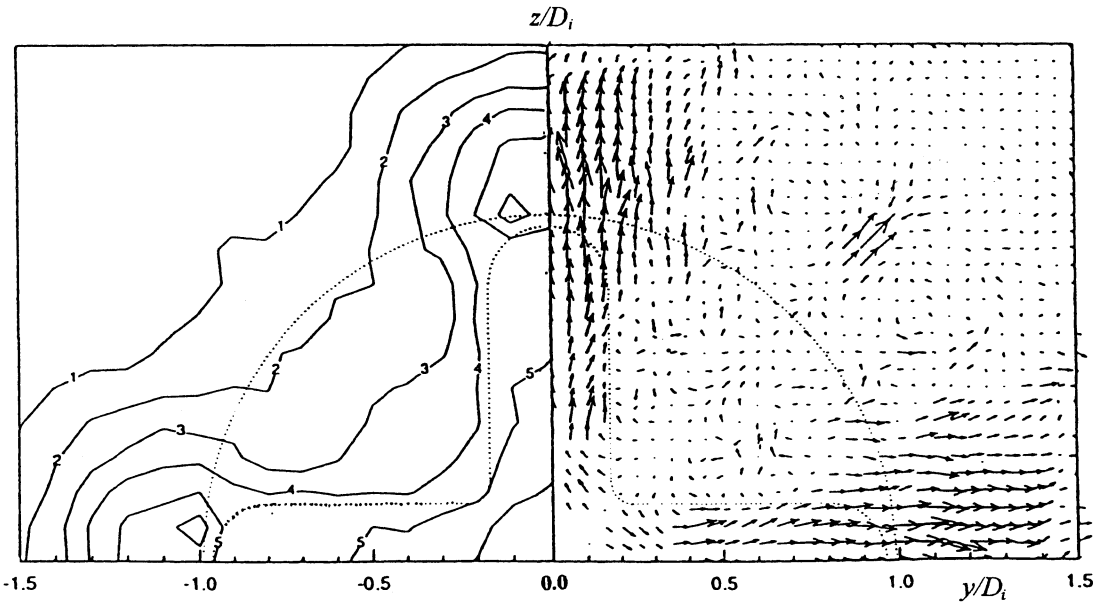

c) $x/D_i = 2.0$

Fig. 6 Contours of the normalized streamwise mean velocity at successive downstream station for $\lambda = 0.4$.

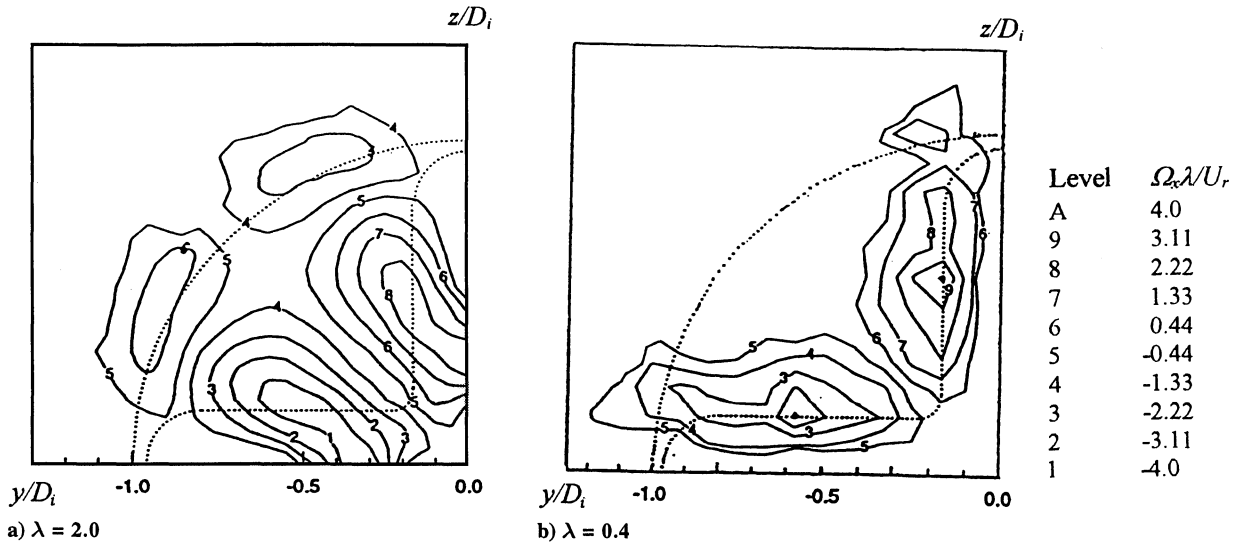

Fig. 7 Contours of the normalized streamwise mean velocity at selected downstream station: $x/D_i = 0.5$.

$\lambda = 2.0$ and 1.1 had become more axisymmetric. For $\lambda = 0.4$, the streamwise mean velocity distribution is still following closely to the projected shape of the four-lobe nozzle. Farther downstream at $x/D_i = 6.0$, the strength of the secondary flow velocity for all cases was reduced further to a negligible level.

Development of the Mean Streamwise Vorticity

The mean streamwise vorticity contours at selected streamwise locations are presented in Fig. 7. As expected, two symmetrical pairs of counter-rotating steamwise vortices are formed behind the trailing edge at $x/D_i = 0.5$ for $\lambda = 2.0$ (Fig. 7a). The size and strength of the vortices shed by the lobe were larger and stronger than those that appeared at the annular wall. The mean streamwise vorticity at both locations maintained nearly the same strength from the trailing edge to about $x/D_i = 1.0$. After $x/D_i = 1.0$ and to the end of the measurement range, the mean streamwise vorticity strength decreased rapidly. It was also observed that the location of the vortices near the annular wall were not stationary but moving away from the plane of symmetry from $x/D_i = 1.0$ onward.

For $\lambda = 0.4$, the size of the streamwise vortices near the trailing edge were slightly smaller (but not weaker) than those of $\lambda = 2.0$ (compare Figs. 7a and 7b). Higher strength of the streamwise vorticity was concentrated along the lobes. For $\lambda = 1.1$ (not shown here), the size of the vortices was larger than those of $\lambda = 0.4$ but of comparable strength. Streamwise vortices were also found near the annular wall, but they were weaker and decayed faster than those of $\lambda = 2.0$. The positions of the streamwise vortices generated by the lobes for all three cases remain at the same locations to the end of the measurements: an obvious effect of confined flows.

The streamwise evolution of the average circulation per vortical structure shown in Fig. 7 is presented in Fig. 8a. The circulation for each vortical structure is evaluated as described earlier. As may be expected, the average circulation for the vortices shed by the lobe for $\lambda = 2.0$ was found to be the highest but decaying rapidly such that by $x/D_i = 5$, the strength had reduced to a negligible level. For the $\lambda = 0.4$ and 1.1 cases, the trailing edge values were not as high as that of $\lambda = 2.0$ but the decay rates were found to be more gradual with downstream distance.

The development for the peak mean streamwise vorticity in Fig. 8b is plotted on a log-log scale. Although the average circulation results showed different forms of decay, results for all cases considered here appeared to fall on the same decaying curve within the range of measurement. The decay of the overall streamwise vorticity was actually faster than that of the peak vorticity. The results thus suggested that the dissipation of the streamwise vortices did not happen abruptly, but rather it appeared to be a gradual process consisting of the breaking down of the large streamwise vortices into many smaller (but not weaker) streamwise vortices. Thus, mixing

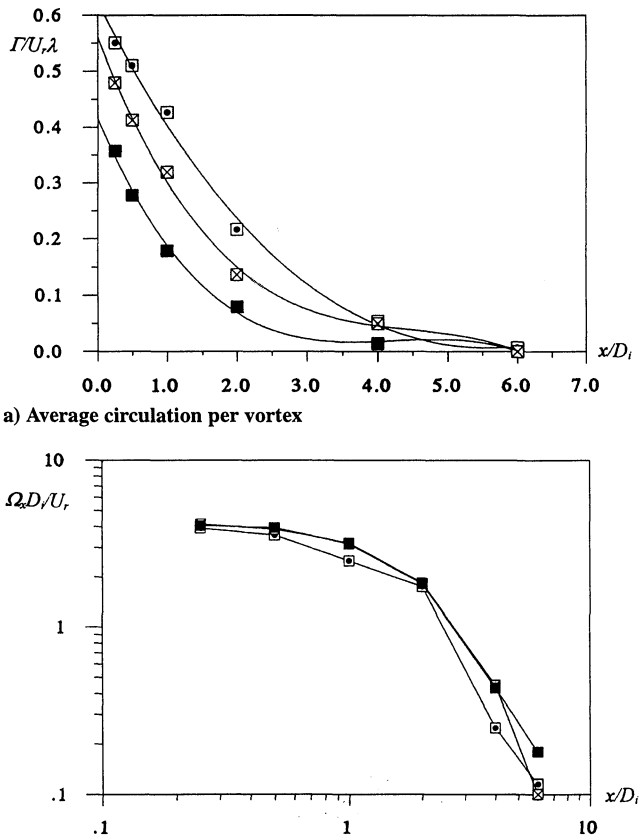

Fig. 8 Variations of the normalized velocity: ⊡, $\lambda = 2.0$; ⊠, $\lambda = 1.1$; and ■, $\lambda = 0.4$.

at a finer scale could be achieved. The results, therefore, agree well with those obtained by Belovich and Samimy.[14]

A schematic of the vortical structure near the trailing edge of the nozzle at $\lambda = 2.0$ and 0.4 may be postulated based on the preceding measurements and is shown in Figs. 9a–9c. As a consequence of the velocity ratio, two azimuthal vortex filaments would be shed immediately behind the trailing edge, one from the inner annular wall with another one from the outer wall of the central lobed nozzle. The two vortex filaments, initially, should be aligned closely to the contours of the annular and lobed nozzle walls (Fig. 9a). Farther downstream, as a result of the streamwise vorticity (Fig. 9b) shed by the lobe and that originated from the gap between the lobe peak and inner annular wall, the two azimuthal vortex filaments would be reoriented

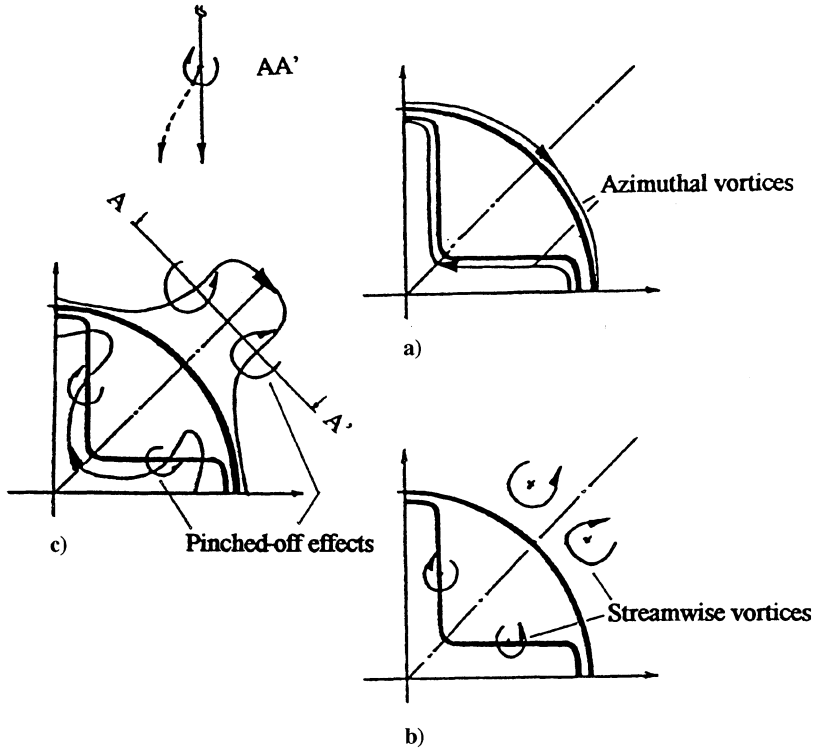

Fig. 9 Schematic of the vortical structure near the trailing edge of the lobed nozzle at $\lambda = 2.0$.

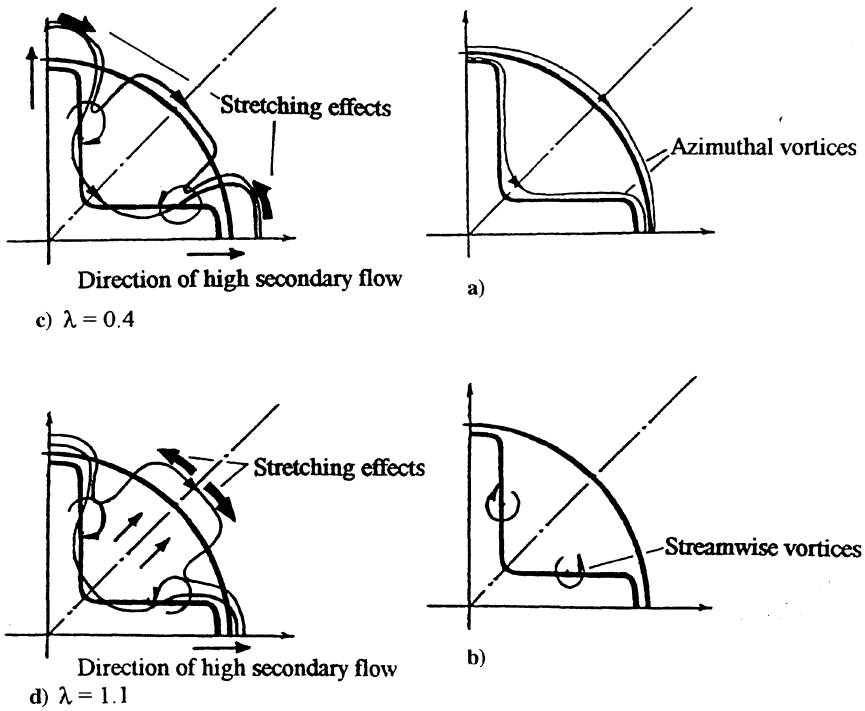

Fig. 10 Schematic of the vortical structure near the trailing edge of the lobed nozzle at $\lambda = 0.4$ and 1.1.

(Fig. 9c). The streamwise vortices generated by the lobes distort the azimuthal vortex filament into a pinched-off effect as described by McCormick and Bennett.[12] An additional pinched-off effect also appears on the azimuthal vortex filament shed at the annular wall. High turbulent kinetic energy would be generated at both pinched-off locations. Furthermore, when the section views along the AA′ plane were considered, it was noted that the azimuthal vorticity was actually riding on the streamwise vortices. The sense of rotation for the azimuthal vorticity would be likely to divert the streamwise vortices in the direction away from the plane of symmetry (Fig. 9c). This may explain the increase in spacing for the streamwise vortices at the annular wall.

For the case of $\lambda = 0.4$ shown in Fig. 10a, the azimuthal vortex filaments were shed at the central lobed nozzle wall and the annular wall. The streamwise vorticity generated by the lobe was confined to within the lobe (Fig. 10b). At farther downstream locations, higher strength of secondary flow along each lobe pushes the azimuthal vortex filament near the lobe peak regions farther to the surrounding area. At the same time, the streamwise vortices at the lobe peaks stretched the azimuthal vortex filament with a consequence of increasing the corresponding strength (through the conservation of angular momentum). As the azimuthal vortex filament is being stretched, high turbulent kinetic energy would be generated and, thereby, enhanced the mixing between the core fluid

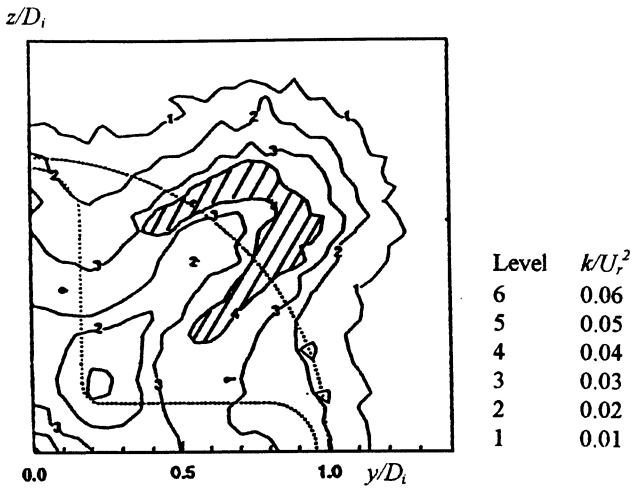

a) $\lambda = 2.0$

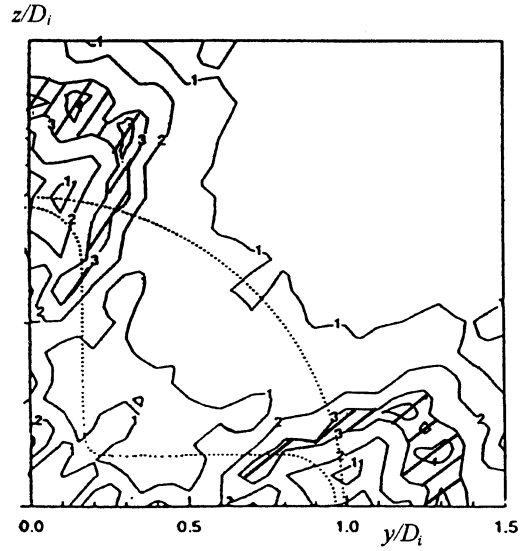

b) $\lambda = 1.1$

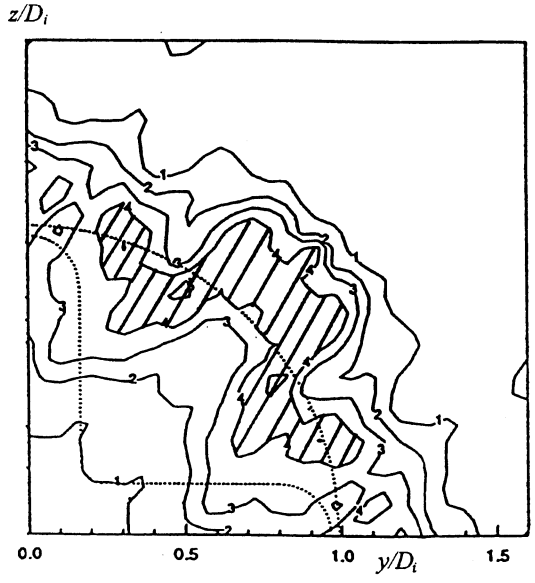

c) $\lambda = 0.4$

Fig. 11 Contours of the normalized turbulent kinetic energy at selected downstream station: $x/D_i = 2.0$.

and the surrounding fluid at the corresponding region (Fig. 10c). Whereas the azimuthal vortex filament near the lobe peaks is being stretched for $\lambda = 0.4$, similar situations also occurred at regions near the plane of symmetry for $\lambda = 1.1$ (Fig. 10d). The difference may be attributed to the higher secondary flow velocity being generated in different outward radial direction (cf., Figs. 5c and 6c).

Development of the Turbulent Kinetic Energy

Turbulent kinetic energy contours at selected downstream stations are shown in Fig. 11 for the $\lambda = 2.0$ case. Higher levels of k appeared initially at the wake of the walls at $x/D_i = 0.5$. Subsequently, streamwise vorticity caused the redistribution of the streamwise velocity contours and higher levels of k began to appear at regions of steep velocity gradients, i.e., at around the straight parallel sidewall of each lobe at $x/D_i = 1.0$. Farther downstream at $x/D_i = 2.0$ and in Fig. 11, additional production of k appears at locations near the annular wall. By the end of the measurement range, the levels of k across the wake in general became higher than those at the locations close to the trailing edge.

For $\lambda = 0.4$ and 1.1, higher levels of k appeared, initially, at the wake of the sidewalls and, subsequently, at regions close to the peak of each lobe, where the stretching effects on the azimuthal vortex filament by the streamwise vorticity existed; see Figs. 11b–11c. This obviously would lead to mixing enhancement at the corresponding regions.

The present investigation shows that the interaction of the azimuthal and streamwise vorticities is responsible for a considerable increase in the mixing process. It is obvious that the streamwise vorticity generated by the lobe geometry is important to enhance the mixing between the two coflowing streams, as in the cases of $\lambda = 1.1$ and 2.0. For the mixing between the core and the surrounding still fluid, different velocity ratios exhibit different forms of mixing. For the case $\lambda = 2.0$, additional streamwise vorticity was generated by the gap between the lobe peaks and annular wall. This had actually enhanced the mixing between the annular flow and the surrounding still fluid. For the case $\lambda = 0.4$, higher strength of the secondary flow generated along each lobe pushes the azimuthal vortex filament farther into the still fluid region. At the same time, the formation of the streamwise vorticity near the lobe peak regions stretches the azimuthal vortex filament. For $\lambda = 1.1$, similar stretching effects appear near the plane of symmetry. Through the conservation of angular momentum, the azimuthal vorticity would be intensified and, hence, produce turbulence and enhance the mixing. It may be also expected that, for a given lobed nozzle configuration and at higher velocity ratio, higher mean shear would result in generating higher level of turbulent kinetic energy and thereby further enhance the mixing rate.

Concluding Remarks

The velocity characteristics of turbulent, confined, coaxial jets with a central lobed mixer have been measured using a two-component fiber-optic laser-Doppler anemometer with initial turbulent boundary layers. The central lobed mixer concerned was a four-lobe nozzle. Tests were conducted at velocity ratios (outer to inner, λ) of 2.0, 1.1, and 0.4, respectively.

At $\lambda = 2.0$, in addition to the generation of the streamwise vorticity that one would expect from the geometry of the lobe, streamwise vorticity was also found to originate between the lobe peaks and the inner annular walls. It is obvious that the former is important to enhance the mixing between the two coflowing streams, whereas the latter is important to the mixing between the annular flow and the surrounding still fluid. In the presence of streamwise vorticity, the flow between the two coflowing streams and that with the surrounding stagnant fluids can actually mix faster than the normal coaxial nozzle arrangement.

At $\lambda = 0.4$, the generation of the streamwise vorticity was by the geometry of the lobe only and was confined at regions near the lobe peaks. The streamwise vorticity deformed and stretched the normal vortex filament shed at the lobe peak regions with a consequence of enhanced mixing with the surrounding still fluid at the corresponding regions. However, the mixing between the core and the annular fluid was not as efficient as in the case of $\lambda = 2.0$, due largely to the weaker strength of secondary flow generated by the lobe geometry.

For the case when the velocities at both streams were almost equal, i.e., at $\lambda = 1.1$, streamwise vorticity generated by the lobes was stronger than that of the $\lambda = 0.4$ case but lower than that of the $\lambda = 2.0$ case. The overall trend of the mixing process, however, was similar to that of the $\lambda = 0.4$ case with the mixing between the core and the surrounding fluid being more efficient than between the two coflowing streams.

In general, in the present confined situation, streamwise vortices generated by the lobes remained within the radial extent of each lobe as they travel downstream. The higher-speed stream generates higher strength of secondary flow, which in turn determines the types of mixing observed. When the core nozzle speed is higher, the mixing between the core and the surrounding fluid would be more efficient. When the annular speed is higher, mixing between the core and the annular fluid would become more efficient.

Acknowledgments

The authors are grateful for the financial support of this project by the Academic Research Grant Committee and a research studentship to X. G. Xu from the School of Mechanical and Production Engineering.

References

[1]Durao, D., and Whitelaw, J. H., "Turbulent Mixing in the Developing Region of Coaxial Jets," *Journal of Fluids Engineering*, Vol. 95, 1973, pp. 467–473.

[2]Ribeiro, M. M., and Whitelaw, J. H., "Turbulent Mixing of Coaxial Jets with Particular Reference to the Near-Exit Region," *Journal of Fluids Engineering*, Vol. 98, 1976, pp. 284–291.

[3]Ribeiro, M. M., and Whitelaw, J. H., "Coaxial Jets With and Without Swirl," *Journal of Fluid Mechanics*, Vol. 96, 1980, pp. 769–795.

[4]Ko, N. W. M., and Kwan, A. S. H., "The Initial Region of Subsonic Coaxial Jets, Part 1," *Journal of Fluid Mechanics*, Vol. 73, 1976, pp. 305–332.

[5]Kwan, A. S. A., and Ko, N. W. M., "The Initial Region of Subsonic Coaxial Jets, Part 2," *Journal of Fluid Mechanics*, Vol. 82, 1977, pp. 273–287.

[6]Champagne, F. H., and Wygnanski, I. J., "An Experimental Investigation of Coaxial Turbulent Jets," *International Journal of Heat and Mass Transfer*, Vol. 14, 1971, pp. 1445–1464.

[7]Zaman, K. B. M. Q., "Spreading Characteristics and Thrust of Jets from Asymmetric Nozzles," AIAA Paper 96-0200, 1996.

[8]Zaman, K. B. M. Q., "Axis Switching and Spreading of an Asymmetric Jet: The Role of Coherent Structure Dynamics," *Journal of Fluid Mechanics*, Vol. 316, 1997, pp. 1–27.

[9]Zaman, K. B. M. Q., Reeder, M. F., and Samimy, M., "Control of an Axisymmetric Jet Using Vortex Generators," *Physics of Fluids A*, Vol. 6, No. 2, 1993, pp. 778–793.

[10]Manning, T. A., "Experimental Studies of Mixing Flows with Streamwise Vorticity," M.S. Thesis, Massachusetts Inst. of Technology, Cambridge, MA, Sept. 1991.

[11]Eckerle, W. A., Sheibani, H., and Awad, J., "Experimental Measurement of the Vortex Development Downstream of a Lobed Forced Mixer," *Journal of Engineering for Gas Turbines and Power*, Vol. 63, 1992, p. 114.

[12]McCormick, D. C., and Bennett, J. C., Jr., "Vortical and Turbulent Structure of a Lobed Forced Mixer Free-Shear Layer," *AIAA Journal*, Vol. 32, No. 9, 1994, pp. 1852–1859.

[13]Yu, S. C. M., and Yip, T. H., "Measurements of Velocities in the Near Field of a Lobed Forced Mixer Trailing Edge," *Aeronautical Journal*, Vol. 101, 1997, pp. 121–129.

[14]Belovich, V. M., and Samimy, M., "Mixing Processes in a Coaxial Geometry with a Central Lobed Mixer Nozzle," AIAA Paper 96-0118, 1996.

[15]Yu, S. C. M., and Xu, X. G., "Turbulent Mixing of Co-Axial Nozzle Flows with a Central Lobed Mixer," *Journal of Propulsion and Power*, Vol. 13, No. 4, 1997, pp. 517–524.

[16]Xu, X. G., "Measurements of Co-Axial Nozzles with a Central Lobed Mixer," M.Eng. Thesis, Thermal and Fluids Engineering Div., School of Mechanical and Production Engineering, Nanyang Technological Univ., Singapore, 1997.

G. Laufer
Associate Editor